Supplemental Material – Scaling theory for athermal fiber network mechanics

Jordan Shivers,[1,2] Sadjad Arzash,[1,2] Abhinav Sharma,[3] and Fred C. MacKintosh[1,2,4]

[1]*Department of Chemical and Biomolecular Engineering, Rice University, Houston, TX 77005, USA*
[2]*Center for Theoretical Biological Physics, Rice University, Houston, TX 77030, USA*
[3]*Leibniz Institute of Polymer Research Dresden, Dresden, Germany*
[4]*Departments of Chemistry and Physics & Astronomy, Rice University, Houston, TX 77005, USA*

Removal of disconnected and dangling clusters

Our reported coordination number z corresponds to the average network coordination after the removal of dangling and disconnected bond clusters, which do not contribute to the network's mechanical response in the zero-frequency limit. Dangling clusters, shown in Fig. S1a, are defined as clusters of bonds connected to the rest of the network by a single bond, or "bridge". Bridges are identified as biconnected components containing only a single bond and subsequently removed, resulting in disconnected clusters. Disconnected clusters, shown in Fig. S1b, are then removed by identifying all connected components in the network and removing all but the largest, corresponding to the bulk network. The Boost graph library [1] is utilized for identification of connected and biconnected components.

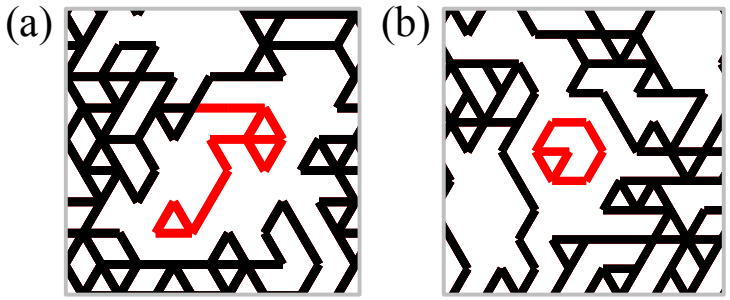

FIG. S1. (a) A dangling cluster (red) is defined as a cluster of bonds connected to the rest of the network by only one bond. These are detected and removed by removing "bridges," bonds which, if cut, disconnect the graph. Bridges are identified as biconnected components containing only one bond. (b) A disconnected cluster (red) is a cluster of bonds that is disconnected from the bulk network. We remove these by identifying all independent connected components and retaining only the largest one.

System-size dependence of the critical strain distribution

We determine the critical shear strain γ_c for each network sample as the strain corresponding to the onset of finite K in the $\kappa = 0$ limit. Consistent with prior work [2], we observe a decrease in the width of the γ_c distribution with increasing system size, as shown in Fig. S2 for triangular networks.

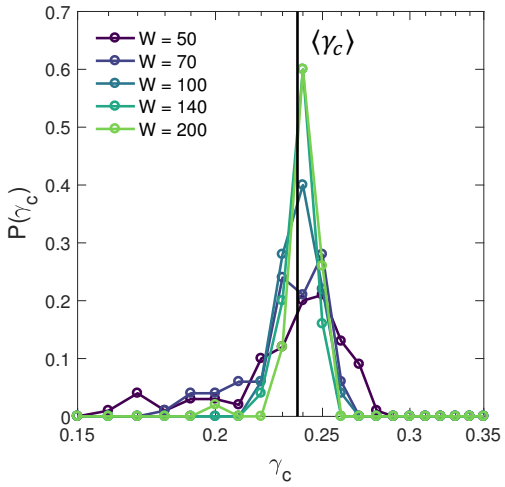

FIG. S2. The probability distribution of the critical strain γ_c decreases in width with increasing system size. These data correspond to triangular networks with $\kappa = 0$ and $z = 3.3$, with at least 50 networks each for each system size. The vertical black line denotes the average γ_c value for networks of size $W = 200$.

Strain-controlled criticality in packing-derived networks

Fig. S3 shows the measured shear stress vs. strain for both triangular and packing-derived networks. A transition from a bending-dominated regime with $\sigma_{xy} \sim \kappa$ to a stretching-dominated regime with $\sigma_{xy} \sim \mu$ occurs at the critical strain γ_c, at which networks with $\kappa = 0$ develop nonzero stress. Figure S4 shows the computed K vs. strain curves as well as the scaling of K with $\Delta\gamma$ for packing-derived networks, with $K \sim |\Delta\gamma|^f$ for $\gamma > \gamma_c$ and $K \sim \kappa|\Delta\gamma|^{f-\phi}$ for $\gamma < \gamma_c$.

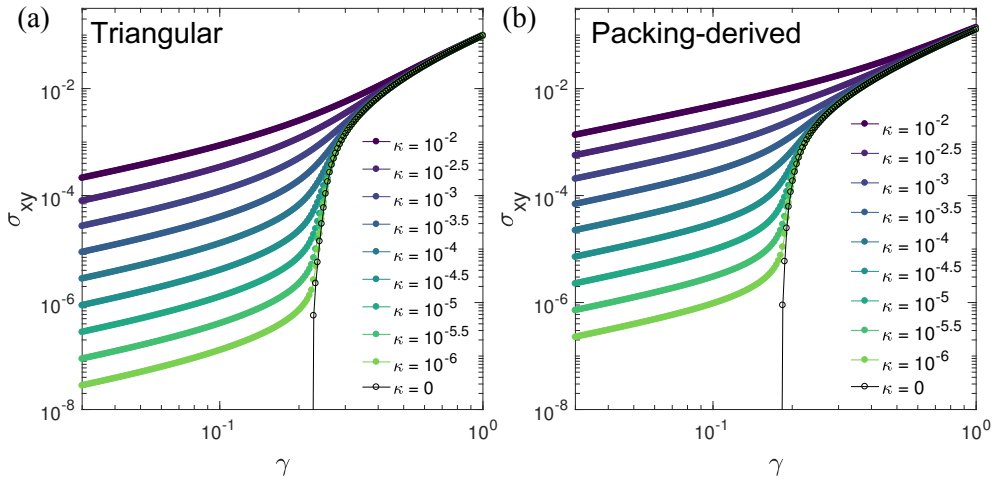

FIG. S3. Shear stress σ_{xy} vs. shear strain γ for (a) triangular networks of size $W = 140$ and (b) packing-derived networks of size $W = 120$, both diluted to $z = 3.3$, with varying reduced bending stiffness κ.

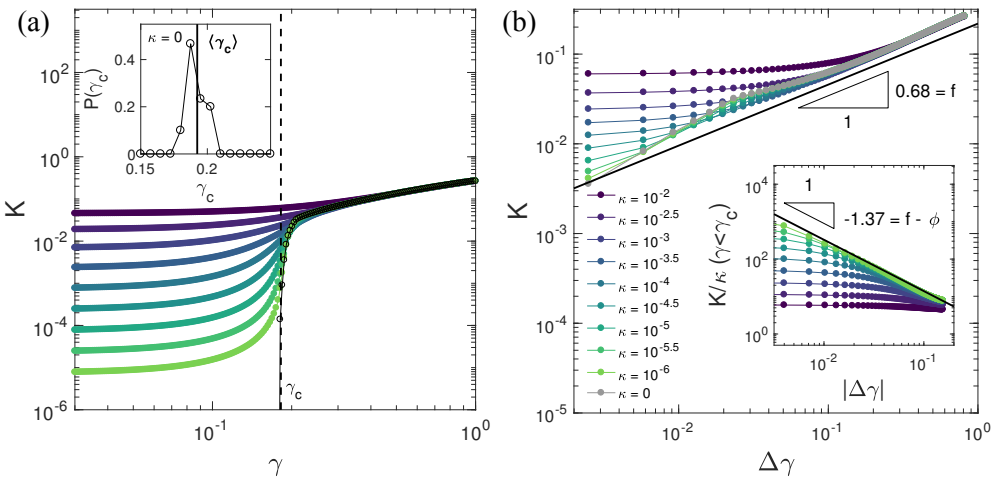

FIG. S4. (a) Differential shear modulus K vs. shear strain for diluted packing-derived networks of size $W = 120$ and connectivity z = 3.3, with varying reduced bending stiffness κ. The dashed line indicates the observed critical strain γ_c for the ensemble. The inset shows the probability distribution for the measured γ_c values for 30 individual network samples with $\kappa = 0$. (b) For $\gamma > \gamma_c$ and with decreasing κ, K converges to the form $K \sim |\gamma - \gamma_c|^f$, with $f = 0.68 \pm 0.04$. These data are for the same networks as in (a). Inset: In the low-κ limit and below γ_c, K/κ converges to a power law in $|\Delta\gamma|$ with exponent $f - \phi \sim -1.37$.

Bending-rigidity dependence of the nonaffine fluctuations

For both triangular and packing-derived networks, finite bending rigidity suppresses nonaffine fluctuations, as shown in Fig. S5a/c. At the critical strain, the nonaffine fluctuations grow with decreasing κ as $\kappa^{(f-\phi)/\phi}$ (see Fig. S5b/d), as predicted by the scaling theory in the main text.

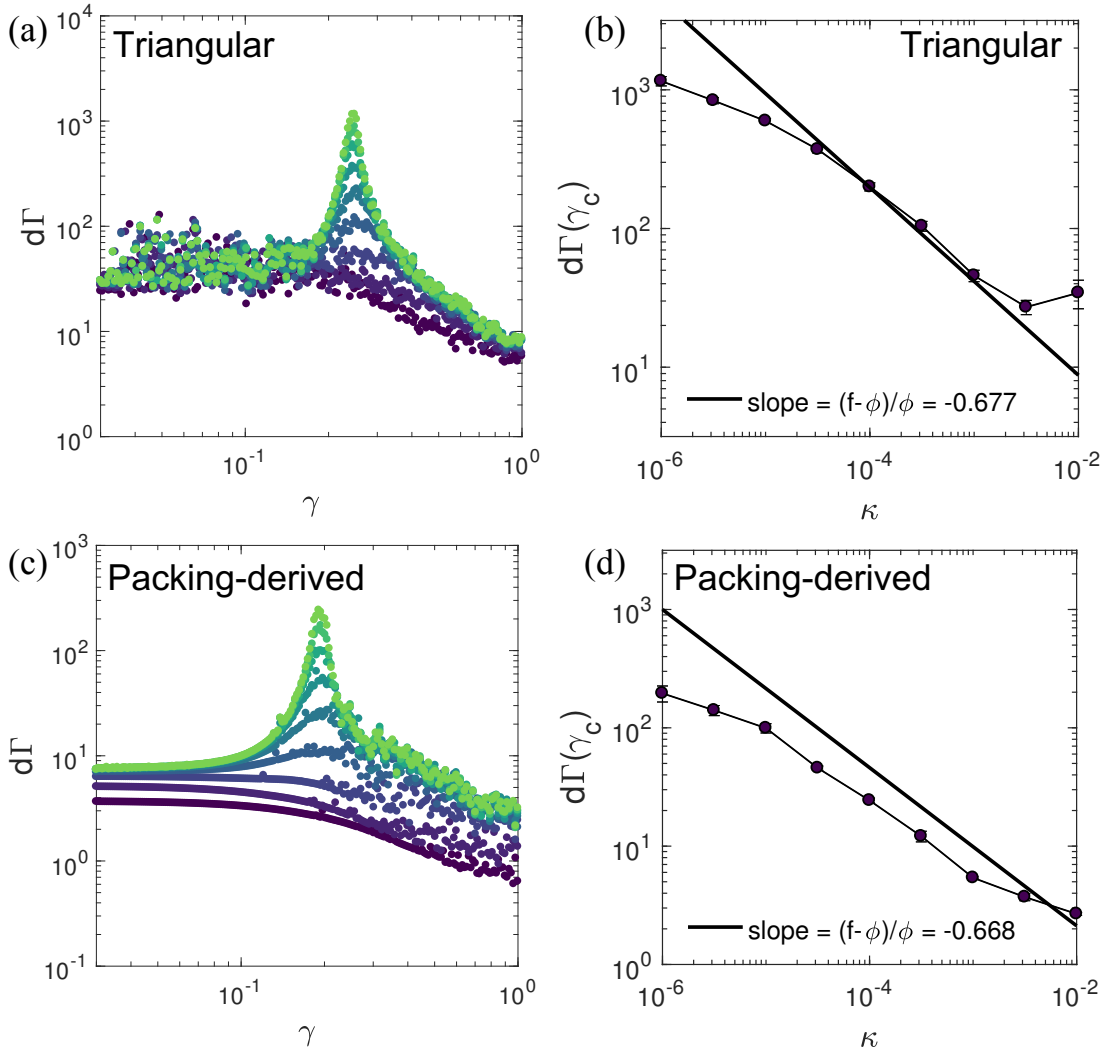

FIG. S5. Differential nonaffinity $d\Gamma$ vs. strain γ for (a) triangular networks of size $W = 140$ and (c) packing-derived networks of size $W = 120$, both with $z = 3.3$ and varying bending rigidity κ. Colors here correspond to those in Figs. 1-3 of the main text. Plotting the values of $d\Gamma$ at the critical strain as a function of κ, we observe reasonable agreement at the inflection point with the predicted scaling $d\Gamma(\gamma_c) \sim \kappa^{(f-\phi)/\phi}$ for both network models (panels b and d) using the f and ϕ values determined independently based on K. Error bars represent standard error of the mean.

Finite-size scaling of the nonaffine fluctuations in networks with finite bending rigidity

We observe that the same finite size scaling of $d\Gamma$ shown for networks with $\kappa = 0$ in Fig. 4 of the main text is also satisfied for networks with small but finite κ, as shown in Fig. S6.

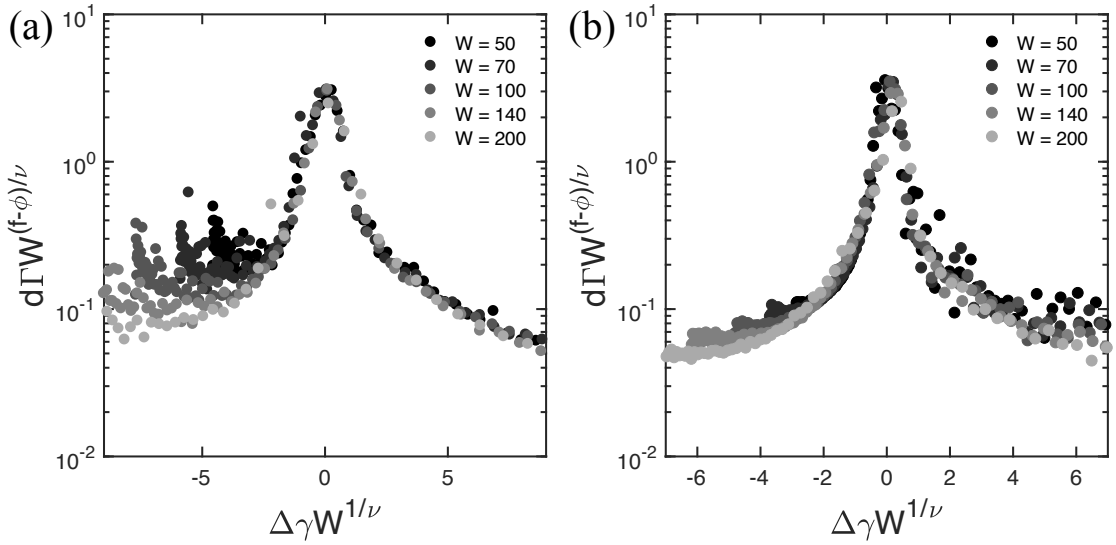

FIG. S6. Plots of $\delta\Gamma/W^{(\phi-f)/\nu}$ vs. $(\gamma-\gamma_c)W^{1/\nu}$ for (a) triangular networks and (b) packing-derived networks with $z = 3.3$ and $\kappa = 10^{-7}$ and varying system sizes demonstrate successful scaling collapse using the f, ϕ, and ν values determined in the main text.

Finite-size scaling from previous work

We demonstrate that while the exponents of $f = 0.75 \pm 0.05$ and $\nu = 2.0 \pm 0.1$ reported for phantom triangular networks in Ref. [3] disagree with our scaling relation $f = 2\nu - 2$, the data used to determine these exponents can be replotted using the predicted ν value of $\nu = (f+2)/d = 1.38$ and with an adjusted value of $\gamma_c(\infty)$ to achieve a reasonable scaling collapse (see Fig. S7).

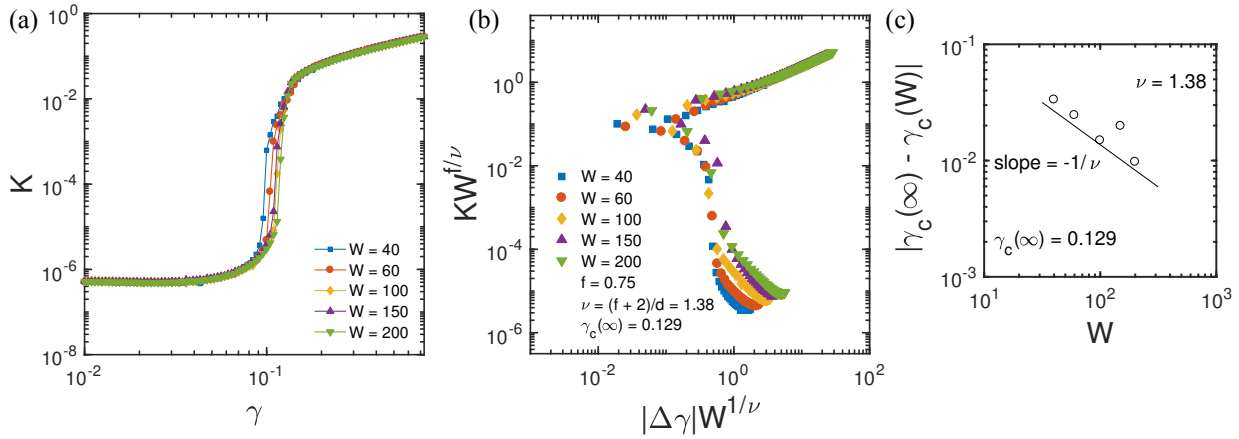

FIG. S7. Data from Ref. [3], replotted with permission. (a) K vs. γ for phantom triangular networks with $z = 3.2$ and varying system size W. (b) The data from the previous panel plotted according to the finite size scaling relation $K \sim W^{-f/\nu}\mathcal{F}_{\pm}\left(|\Delta\gamma|W^{1/\nu}\right)$, using $f = 0.75$, $\nu = (f+2)/d = 1.38$, and $\gamma_c(\infty) = 0.129$. We observe reasonable collapse, comparable to that shown in Ref. [3]. (c) The scaling of $|\gamma_c(\infty) - \gamma_c(W)|$ vs. W using this modified value of $\gamma_c(\infty)$ shows agreement with the predicted scaling of $|\gamma_c(\infty) - \gamma_c(W)| \sim W^{-1/\nu}$.

Stress tensor calculation

For a system with point-like elements with positions $\mathbf{u}_i$, the stress tensor $\boldsymbol{\sigma}$ can be expressed as follows [4, 5]:

$$\sigma_{\alpha\beta} = -\frac{1}{A}\sum_i f_{i,\alpha} u_{i,\beta} \tag{S1}$$

in which the sum is taken over all nodes i, $\mathbf{f}_i = -\partial\mathcal{H}/\partial\mathbf{u}_i$ is the total force exerted on node i, and A is the system's area (or volume in 3D). Eq. S1 can equivalently be expressed as

$$\sigma_{\alpha\beta} = \frac{1}{2A}\sum_{ij} f_{ij,\alpha} u_{ij,\beta} \tag{S2}$$

in which the sum is taken over all pairs of nodes i and j, $\mathbf{u}_{ij} = \mathbf{u}_j - \mathbf{u}_i$, and the force on node i due to its interactions with node j is

$$\mathbf{f}_{ij} = \frac{\partial\mathcal{H}}{\partial\mathbf{u}_{ij}} = \frac{\partial\mathcal{H}}{\partial u_{ij}}\frac{\partial u_{ij}}{\partial\mathbf{u}_{ij}} = \frac{\partial\mathcal{H}}{\partial u_{ij}}\frac{\mathbf{u}_{ij}}{u_{ij}}, \tag{S3}$$

satisfying $\mathbf{f}_i = \sum_j \mathbf{f}_{ij}$ and $\mathbf{f}_{ij} = -\mathbf{f}_{ji}$. While $\mathcal{H}$ may be composed of many-body potentials, the decomposition of $\mathbf{f}_i$ into (pairwise) central forces $\mathbf{f}_{ij}$ shown in Eq. S3 is possible if $\mathcal{H}$ is continuously differentiable [6, 7]. Several prior studies have demonstrated computation of the stress tensor in systems with many-body potentials using this central force decomposition [8–10].

Additionally, one can compute the components of the stress tensor using the principle of virtual work, by manually taking derivatives of $\mathcal{H}$ with respect to the various shear and normal strains:

$$\sigma_{xz} = \frac{1}{A}\frac{\partial\mathcal{H}}{\partial\gamma} \tag{S3}$$

$$\sigma_{xx} = \frac{1}{A}\frac{\partial\mathcal{H}}{\partial\varepsilon_x} \tag{S4}$$

$$\sigma_{zz} = \frac{1}{A}\frac{\partial\mathcal{H}}{\partial\varepsilon_z} \tag{S5}$$

in which γ is simple shear strain and ε_x and ε_z are uniaxial strains along the x and z axes, respectively. We have verified that these methods yield equivalent $\boldsymbol{\sigma}$ within numerical error.

[1] *The Boost Graph Library: User Guide and Reference Manual* (Addison-Wesley Longman Publishing Co., Inc., Boston, MA, USA, 2002).
[2] M. F. J. Vermeulen, A. Bose, C. Storm, and W. G. Ellenbroek, Physical Review E **96**, 053003 (2017).
[3] A. Sharma, A. J. Licup, K. A. Jansen, R. Rens, M. Sheinman, G. H. Koenderink, and F. C. MacKintosh, Nature Physics **12**, 584 (2016).
[4] R. G. Larson, *The Structure and Rheology of Complex Fluids* (Oxford University Press, New York, 1999).
[5] M. Doi and S. F. Edwards, *The Theory of Polymer Dynamics* (Clarendon Press, 1988).
[6] N. C. Admal and E. B. Tadmor, Journal of Elasticity **100**, 63 (2010).
[7] T. J. Delph, Modelling and Simulation in Materials Science and Engineering **13**, 585 (2005).
[8] T. Ishikura, T. Hatano, and T. Yamato, Chemical Physics Letters **539-540**, 144 (2012).
[9] Y. Fu and J.-H. Song, The Journal of Chemical Physics **141**, 54108 (2014).
[10] A. T. Fenley, H. S. Muddana, and M. K. Gilson, PLoS ONE **9**, e113119 (2014).